Use of Synergistic Interactions to Fabricate Strong, Tough, and Conductive Artificial Nacre Based on Graphene Oxide and Chitosan

Sijie Wan,[†,§] Jingsong Peng,[†,§] Yuchen Li,[‡,§] Han Hu,[†,§] Lei Jiang,[†] and Qunfeng Cheng*[,†]

[†]Key Laboratory of Bio-inspired Smart Interfacial Science and Technology of Ministry of Education, School of Chemistry and Environment, BeiHang University, Beijing 100191, People's Republic of China and [‡]Beijing Engineering Research Center of Printed Electronics, Beijing Institute of Graphic Communication, Beijing 102600, People's Republic of China. [§]S. Wan, J. Peng, Y. Li, and H. Hu contributed equally to this work.

ABSTRACT Graphene is the strongest and stiffest material, leading to the development of promising applications in many fields. However, the assembly of graphene nanosheets into macro-sized nanocomposites for practical applications remains a challenge. Nacre in its natural form sets the "gold standard" for toughness and strength, which serves as a guide to the assembly of graphene nanosheets into high-performance nanocomposites. Here we show the strong, tough, conductive artificial nacre based on graphene oxide through synergistic interactions of hydrogen and covalent bonding. Tensile strength and toughness was 4 and 10 times higher, respectively, than that of natural nacre. The exceptional integrated strong and tough artificial nacre has promising applications in aerospace, artificial muscle, and tissue engineering, especially for flexible supercapacitor electrodes due to its high electrical conductivity. The use of synergistic interactions is a strategy for the development of high-performance nanocomposites.

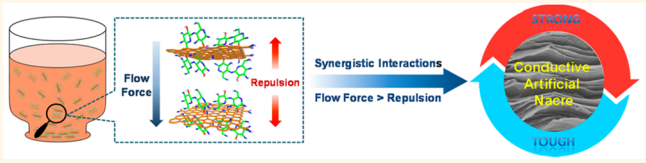

KEYWORDS: artificial nacre · graphene oxide · chitosan · synergistic interaction

Graphene oxide (GO) with many functional groups on its surface[1] is an ideal candidate for the fabrication of artificial nacre.[2−5] High-performance GO-based artificial nacres have been constructed through the use of different kinds of interface interactions such as ionic bonding,[6,7] hydrogen bonding,[8−10] covalent bonding,[11−15] and $\pi-\pi$ conjugated interactions.[16] Although the strength and stiffness of these materials are significantly higher than those of natural nacres,[17] GO-based artificial nacres are disadvantaged by reduced ductility or toughness. Thus, obtaining integrated strength and toughness in GO-based artificial nacre has remained a great challenge.

The extraordinary properties of natural nacre are, in fact, attributed to the synergistic toughening effects from different building blocks and interface interactions.[18] Recently, we demonstrated integrated strength and toughness in graphene oxide-based artificial nacre through the use of synergistic building blocks: graphene oxide (GO)/molybdenum disulfide (MoS_2)/thermoplastic polyurethanes (TPU).[19]

Herein, we demonstrate the construction of integrated, strong and tough, GO-based artificial nacre through synergistic interactions of hydrogen and covalent bonding. The tensile strength and toughness of this artificial nacre reach 526.7 MPa and 17.7 MJ/m^3, which is 4 and 10 times higher, respectively, than that of natural nacre.[17] Meanwhile, the electrical conductivity of the artificial nacre was measured as high as 155.3 S/cm, which is promising for applications in aerospace, flexible supercapacitor electrodes, artificial muscle, and tissue engineering. This strategy of using synergistic interactions offers a new avenue for the development of high-performance, integrated, bioinspired nanocomposites.

RESULTS AND DISCUSSION

Chitosan (CS),[20] a biodegradable material, is an ideal "soft" component for constructing artificial nacre due to its many hydroxyl and amine functional groups. The manufacturing

* Address correspondence to cheng@buaa.edu.cn.

Received for review May 13, 2015 and accepted September 7, 2015.

Published online September 07, 2015
10.1021/acsnano.5b02902

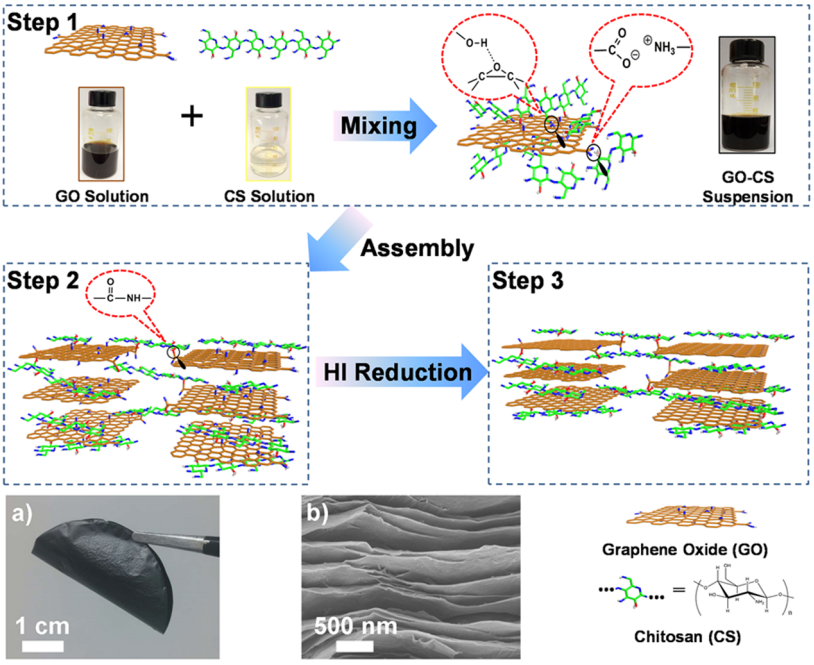

Scheme 1. Illustration of the manufacturing process of rGO-CS artificial nacres. Step 1: The GO−CS hybrid building blocks are achieved through mixing GO solution and CS solution with alkali. Step 2: GO-CS hybrid building blocks are assembled into GO-CS-based nanocomposites through vacuum-assisted filtration. Step 3: After HI reduction, the artificial nacres rGO-CS are obtained. A digital photograph (a) and a cross-section SEM image (b) of rGO-CS-V artificial nacre are shown.

TABLE 1. GO Content and the Electrical Conductivity of HI-Reduced GO and GO-CS-Based Nanocomposites

sample	input GO content (wt %)	GO content by TGA (wt %)	electrical conductivity after HI reduction (S/cm)
GO			223.3 ± 23.0
GO-CS-I	70	68.7	34.6 ± 11.4
GO-CS-II	75	73.2	56.6 ± 5.8
GO-CS-III	80	78.3	62.9 ± 16.9
GO-CS-IV	90	89.3	140.4 ± 8.8
GO-CS-V	95	94.4	155.3 ± 4.0

process of the artificial nacre is shown in Scheme 1. In step 1, the GO solution was mixed with CS solution to achieve hybrid building blocks of GO nanosheets coated with CS (GO-CS).[21−28] In step 2, these hybrid building blocks were assembled into GO-based nanocomposites through vacuum-assisted filtration. In step 3, the artificial nacres were obtained by chemically reducing GO-CS-based nanocomposites with hydroiodic acid (HI). A series of GO-CS-based nanocomposites with different GO contents were designated as GO-CS-I, GO-CS-II, GO-CS-III, GO-CS-IV, and GO-CS-V. The exact GO contents, determined by thermogravimetric analysis (TGA), are shown in Table 1. The corresponding curves are shown in Figure S1. In addition, GO-CS-based nanocomposite control samples with the same CS content as the GO-CS-V nanocomposite were fabricated through evaporation-induced self-assembly. They are designated as GO-CS-E and shown in Table S1.

The fabrication of hybrid building blocks of GO-CS with high GO content is very difficult to achieve through simple mixing. That is why, until now, there have been no reports on GO-CS-based nanocomposites with high GO content. Here, we describe a simple and efficient approach developed to solve this problem. Drops of CS solution are slowly delivered into the GO solution, until a precipitate gel appears.[29] An alkali is added to the mixing solution to adjust the charge distribution on the GO nanosheets and CS molecules.[30] Using sonication for about 30 min, the precipitate gel is dispersed into the homogeneous suspension. With the CS content increasing, the GO nanosheets are absorbed with more CS molecules through hydrogen bonding. Intramolecular hydrogen bonding also occurs between CS molecular chains, resulting in a notable increase in the thickness of the hybrid building blocks, as confirmed by atomic force microscopy (AFM), shown in Figure S2.

X-ray diffraction (XRD) results (Figure 1a) show that the *d*-spacing distance increases from 8.52 Å for the pure GO film to 8.72 Å for the GO-CS-V nanocomposite (Table S2), demonstrating that the CS was successfully inserted into the GO nanosheets to form the uniform layered nacre-like structure. Additionally, the broad plateaus and multitude of peaks with 2θ values in the range 10−25° were just observed for the other GO-CS nanocomposites, indicating disordered structure of these nanocomposites. The corresponding cross-section morphology of GO-CS-based and rGO-CS nanocomposites is shown in Figures S3 and S4. The Fourier

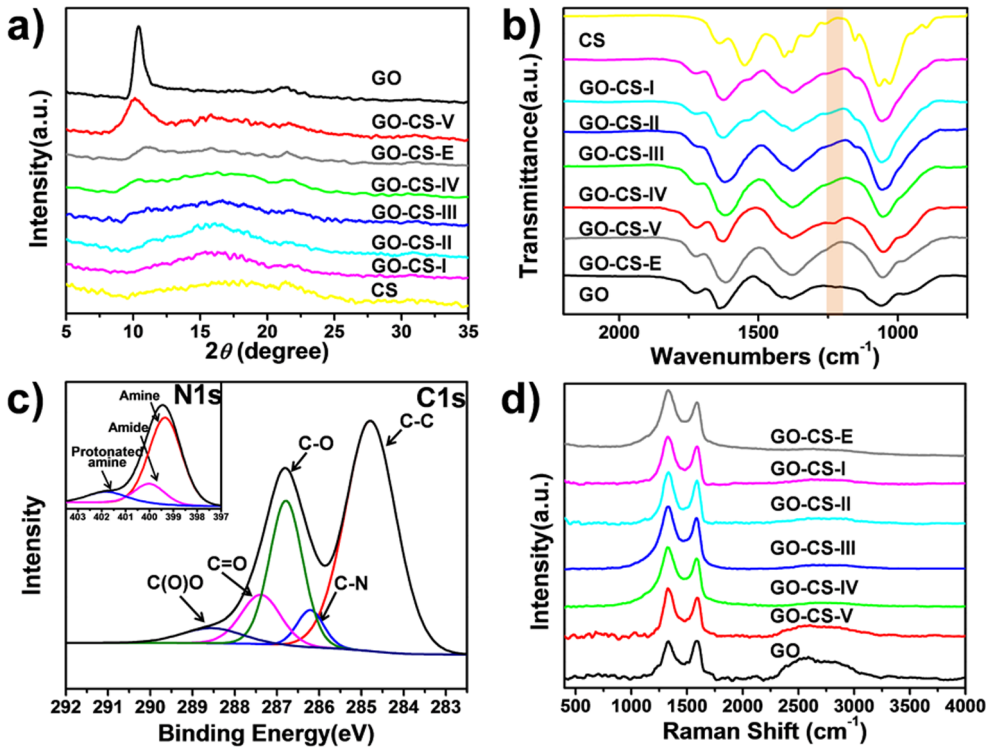

Figure 1. XRD pattern of GO-CS nanocomposites (a) indicating the degree of order for the lamellar nanocomposite structure. FTIR spectra of GO-CS nanocomposites (b) illustrate successful covalent reaction of GO-CS-V for the increase of peak intensity at 1227 cm^{-1}. (c) XPS spectrum of GO-CS-V, showing the increase of peak intensity of C−N and amide, indicating a covalent reaction between GO and CS. The broad peak of C_{1s} can be fitted into five peaks at 284.7, 286.2, 286.8, 287.4, and 288.6 eV, corresponding to C−C, C−N, C−O, C═O, and C(O)O. The broad peak of N_{1s} can be fitted into three peaks at 399.4, 400.0, and 401.8 eV, corresponding to amine, amide, and protonated amine groups. (d) Raman spectra of GO-CS nanocomposites. The I_D/I_G ratios are listed in Table S3.

transform infrared (FTIR) spectra (Figure 1b) show that the characteristic absorption at 1261 cm^{-1}, attributed to the stretch vibration of the C−N of not fully deacetylated amide groups of CS, red-shifts to 1227 cm^{-1} and significantly intensifies only in the GO-CS-V nanocomposite, indicating that the amidation occurred between GO nanosheets with CS molecules. The X-ray photoelectron spectroscopy (XPS) results of the GO-CS-V nanocomposite (Figure 1c) show that the peak intensity of C−N and amide groups is increased and the peak intensity of protonated amine and amine groups of GO-CS-V decreases in comparison with GO-CS-E nanocomposites (Figure S5), further confirming that many more amine groups transferred into amide groups after chemical reaction in the GO-CS-V nanocomposite. The Raman spectra are shown in Figure 1d, and the corresponding I_D/I_G ratios are listed in Table S3.

To further explore the chemical reaction between GO and CS in GO-CS-V nanocomposites, a mechanism of flow force effect is proposed, as shown in Figure 2. For GO-CS hybrid building blocks with low CS content, the flow force in the vacuum-filtration process would facilitate spreading of the CS molecular chains, resulting in the formation of intermolecular hydrogen bonding between GO and CS. On the other hand, if the steric

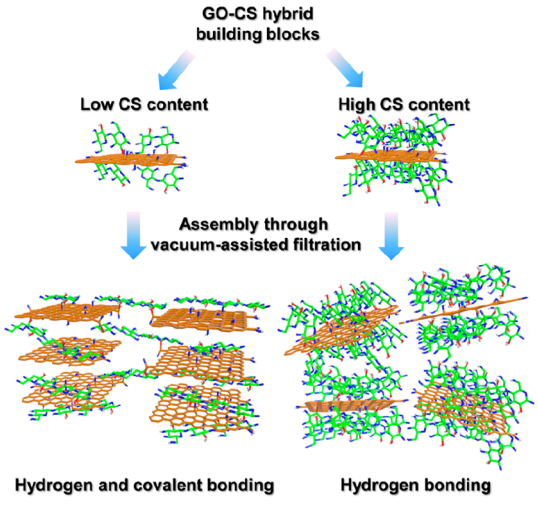

Figure 2. Proposed mechanism: For GO-CS hybrid building blocks with low CS content, the flow force in the filtration process results in the spreading of CS molecular chains along the GO nanosheets and the formation of intermolecular hydrogen bonding between GO and CS. On the other hand, the buried reaction sites (amine) distributed on the CS are exposed and chemically react with carboxyl groups on the GO nanosheets, leading to covalent bonding between GO and CS. By contrast, for the GO-CS hybrid building blocks with high CS content, "electrosteric stabilization" leads to strong repulsion, resulting in only hydrogen bonding in the GO-CS-based nanocomposites.

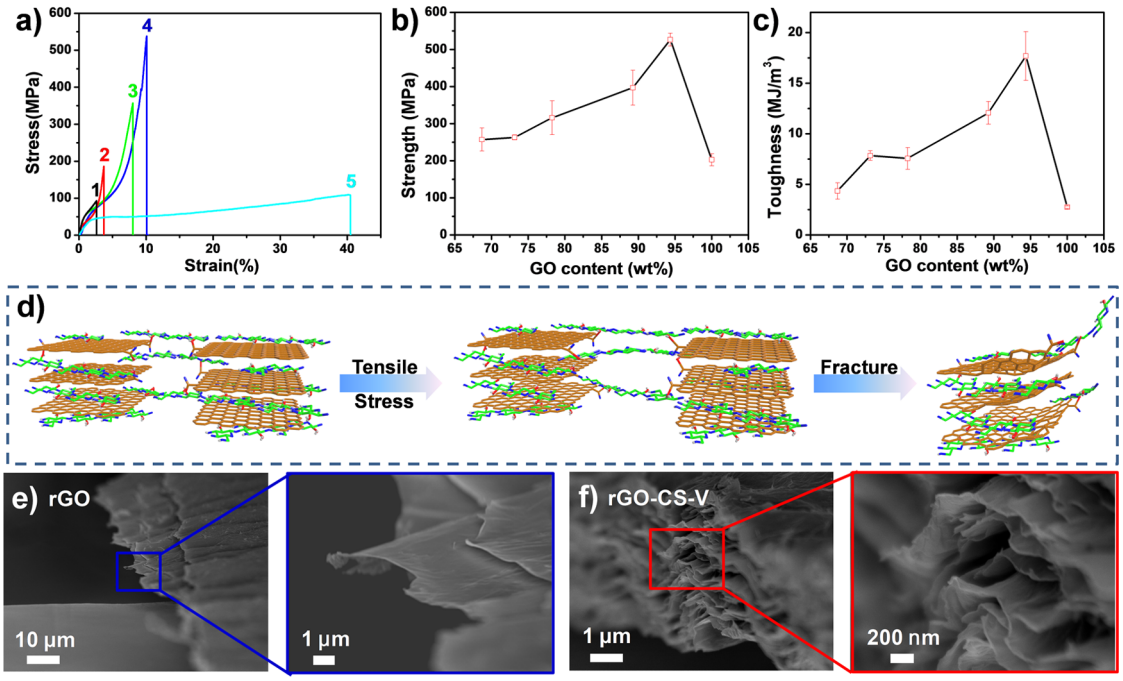

Figure 3. Stress−strain curves (a) of GO films (curve 1), rGO films (curve 2), GO-CS-V nanocomposites (curve 3), rGO-CS-V artificial nacre (curve 4), and CS films (curve 5). Tensile strength (b) and toughness (c) of the rGO-CS artificial nacre with different GO content. Proposed fracture process (d) of rGO-CS-V artificial nacre. The curled long chain of CS is gradually stretched and broken under loading, resulting in curving of the edges of the rGO nanosheets. SEM lateral view profiles of fractured surfaces of rGO films (e) and rGO-CS-V artificial nacre (f) show different fracture morphologies. Compared with the rGO films, the rGO nanosheets of rGO-CS-V artificial nacre are pulled out and curved owing to the breaking of the hydrogen and covalent bondings between rGO and CS molecules.

hindrance of CS is dramatically weakened, then the buried reaction sites (amine) distributed on the CS are exposed and chemically react with carboxyl groups on the GO nanosheets. The characteristic peak of generated amide group at 1227 cm^{-1} appears only in the GO-CS-V nanocomposite as shown in Figure S6, which is direct evidence of covalent cross-linking between GO and the chitosan molecule. On the other hand, the covalent cross-linking could also be further confirmed by XPS, as shown in Figure 1c and Figure S5a. The XPS results of the GO-CS-V nanocomposite (Figure 1c) show that the peak intensity of the C−N and amide groups is increased and the peak intensity of protonated amine and amine groups of GO-CS-V decreases compared with the GO-CS-E nanocomposite (Figure S5a), further demonstrating that many more amine groups transferred into amide groups after chemical reaction in the GO-CS-V nanocomposite. By contrast, for GO-CS hybrid building blocks with high CS content, "electrosteric stabilization"[31−33] leads to strong repulsion. As a result, during the assembly process the distribution of the coiled CS with intramolecular hydrogen bonding on the GO nanosheets is very difficult to achieve. A chemical reaction between GO nanosheets and CS cannot occur, and therefore the primary interface interaction is hydrogen bonding.

The typical tensile stress−strain curves of rGO-CS nanocomposites are shown in Figure 3a. Tensile strength and toughness of rGO-CS-V artificial nacre are significantly improved from 106.3 MPa and 1.7 MJ/m^3 for the GO film to 526.7 MPa and 17.7 MJ/m^3, respectively, corresponding to almost 400% improvement in tensile strength compared to the pure CS film (107.3 MPa, curve 5). The mechanical properties of other rGO-CS nanocomposites with different GO content are shown in Figure 3b and c. Optimized rGO-CS-V with a GO content of about 94.36 wt % showed the highest mechanical properties, which are very similar to those of natural nacre with 95 vol % inorganic $CaCO_3$,[17] thus demonstrating the superiority of this bioinspired fabrication strategy. According to our proposed mechanism, there are numerous intramolecular hydrogen bonds in the rGO-CS nanocomposites with high CS content, which decrease the friction between GO nanosheets and show low mechanical properties, especially for toughness. Detailed mechanical properties of GO-CS and rGO-CS nanocomposites are listed in Table S4.

Obviously, the high mechanical properties of rGO-CS-V artificial nacre are attributed to synergistic interactions of hydrogen and covalent bonding, which are clearly demonstrated in the stress−strain curve, as shown in Figure S7a. The cyclic loading experiments were conducted on the rGO-CS-V artificial nacre, and the stress−strain curve is shown in Figure S8. During stage I, the rGO-CS-V artificial nacre shows elastic deformation[4] within a strain of 0.5% reversible deformation, as shown in Figure S8a. With increased loading, the plastic deformation takes place in stage II due to

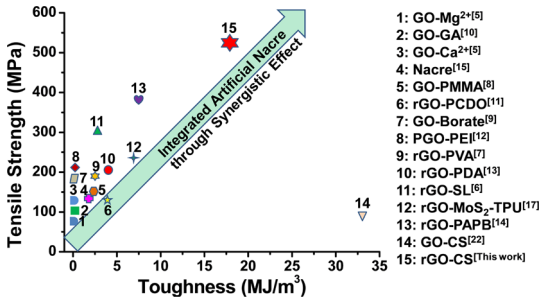

Figure 4. Mechanical properties of natural nacre and other GO-based nanocomposites are compared with rGO-CS-V artificial nacre toughened through synergistic interactions. The rGO-CS-V artificial nacre shows integrated high tensile strength and toughness compared with other GO-based nanocomposites, such as hydrogen bonding of GO-PMMA, rGO-PVA, and rGO-SL, ionic bonding of GO-Mg^{2+}, GO-Ca^{2+}, and GO-Fe^{3+}, $\pi-\pi$ conjugated interactions of rGO-PAPB, covalent bonding of GO-GA, GO-borate, PGO-PEI, rGO-PCDO, and rGO-PDA, and other GO-CS nanocomposites with low GO content.

slippage of GO nanosheets, as shown in Figure S8b. For example, the rGO-CS-V artificial nacre was elongated with a permanent deformation of 0.52% after five successive loading−unloading cycles within a strain of 5%. The intermolecular hydrogen bonding between GO and CS is broken and re-formed in the slippage process, which absorbs much more energy. As loading increases during stage III, the permanent deformation reaches a larger deformation of 2.56% after five successive loading−unloading cycles, as shown in Figure S8c. When further increasing the loading, the covalent bonding is broken, leading to high fracture strength and curling of GO nanosheets compared to the pure rGO film. The proposed fracture mechanism is shown in Figure 3d, and the lateral view profiles of the fracture morphology of the rGO film and rGO-CS-V artificial nacre are shown in Figure 3e and f. The fracture morphologies of the rGO film and rGO-CS-V artificial nacre are shown in Figure S9. The obvious substantial curling of reduced GO nanosheets in the rGO-CS-V artificial nacre can be observed compared to the rGO film. This mode of synergistic interactions for absorbing energy would simultaneously improve the tensile strength and toughness. The other GO-CS-based nanocomposites show only stages I and II in the stress−strain curves, as illustrated in Figure S7b, for GO-CS-I nanocomposite.

As shown in Figure 4, the toughening of artificial nacre through synergistic interactions offers the advantage of integrated strength and toughness when compared with natural nacre and other GO-based nanocomposites, such as hydrogen bonding (GO-PMMA,[10] rGO-PVA,[9] and rGO-SL.[8]), ionic bonding (GO-Mg^{2+},[7] GO-Ca^{2+},[7] and GO-Fe^{3+} [6]), $\pi-\pi$ conjugated interactions (rGO-PAPB[16]), and covalent bonding (GO-GA,[12] GO-borate,[11] PGO−PEI,[14] rGO-PCDO,[13] and rGO-PDA[15]). On the other hand, although the GO-CS nanocomposites with low GO content (1 wt %) show low tensile strength, the toughness is very high. The dramatic improvment of mechanical properties was ascribed to both the interaction between GO and CS and the change in crystallinity.[22] Detailed mechanical properties of natural nacre and GO-based nanocomposites are listed in Table S5. A comparison of GO-based artificial nacre with the synergistic building blocks of rGO-MoS_2-TPU[19] shows that synergistic interactions play a key role in improving the mechanical properties. The tensile strength and toughness of rGO-CS-V is 2.2 and 2.6 times higher, respectively, than that of rGO-MoS_2-TPU (tensile strength of 235 MPa and toughness of 6.9 MJ/m^3).

Furthermore, the high electrical conductivity of rGO-CS-V artificial nacre, measured at 155.3 S/cm (Table 1), is comparable with that in previously reported papers.[34] The use of rGO-CS-V artificial nacre as a conducting wire in a circuit is demonstrated in a video (Movie S1), in which a red LED remains steadily lit while the artificial nacre is bent, indicating a potential application for it in flexible devices.

CONCLUSION

Natural nacre sets a "gold standard" for materials by having both high strength and toughness. Inspired by the natural nacre, we have fabricated artificial nacre based on graphene oxide and chitosan with almost the same ratios of inorganic and organic components in nacre, and this artificial nacre successfully integrates toughness and strength. Our finding is that the synergistic interactions of hydrogen and covalent bonding in this artificial nacre resulted in extraordinary mechanical properties, with tensile strength and toughness 4 and 10 times higher, respectively, than that of natural nacre. This integrated artificial nacre is promising for applications in many fields, such as aerospace, artificial muscles, tissue engineering, and especially flexible supercapacitor electrodes due to its high electrical conductivity. The use of synergistic interactions for toughening artificial nacres can serve as the basis of an alternative strategy for the construction of integrated, high-performance, GO-based nanocomposites in the future.

METHODS

Materials. Graphene oxide was prepared by a modified Hummer's method. Chitosan (medium molecular weight, 75−85% deacetylated) and 57 wt % HI were purchased from Sigma-Aldrich.

Preparation of GO-CS Hybrid Building Blocks. The CS was dispersed in 2% acetic acid solution with a concentration of 10 mg/mL and stirred for 24 h. The GO was dispersed in deionized water with a concentration of 0.5 mg/mL and stirred for 2 h, followed by CS solution addition with different GO/CS ratios under continuous

stirring. Subsequently, a suspension of GO-CS hybrid building blocks was sonicated for 30 min, and some alkali was added to stabilize these suspensions.

Preparation of rGO-CS Nanocomposites. Vacuum filtration was applied to assemble the homogeneous suspension of GO-CS hybrid building blocks into GO-CS nanocomposites. Then, GO-CS nanocomposites were chemically reduced by hydroiodic acid for 6 h, and rGO-CS nanocomposites were obtained.

Characterization. Mechanical properties were conducted *via* a Shimadzu AGS-X Tester with a loading rate of 1 mm/min under a 20 N load cell. All measurements were conducted at room temperature, and all specimens were dried for 24 h at 45 °C before testing. The samples were cut into strips with a width of 3 mm and length of 10 mm, and the thickness of all samples was calculated by scanning electron microscopy (SEM). The Young's modulus of all samples was determined by the slope of the linear region of the stress−strain curves. The toughness was calculated by the area under the stress−strain curves. The mechanical properties for each sample are based on the average value of 3−5 specimens. SEM images were recorded by a Hitachi S-4800 at 1−1.5 kV after sputtering a thin Pt/Au coating onto the samples. AFM was conducted by a Leica TCS SP5. The well-dispersed GO/CS solution was diluted with 100 times pure deionized water. Then, the diluted GO/CS dispersion was dropped on freshly cleaved mica and dried at room temperature to obtain the samples for the AFM measurement. The pure GO nanosheet sample for AFM testing was prepared in the same manner. TGA was performed on a TG/DTA6300, NSK with a temperature increase rate of 10 K/min under nitrogen from 30 to 800 °C. The calculation of GO weight fraction in GO-CS nanocomposites is shown in the Supporting Information. Raman spectroscopy measurements were taken using a Lab-RAM HR800 (Horiba JobinYvon) with an excitation energy of 1.96 eV (633 nm). XPS measurements were carried out in an ESCALab220i-XL (ThermoScientific) using a monochromatic Al Ka X-ray source. X-ray diffraction profiles were taken with Cu Kα radiation ($\lambda = 1.54$ nm). The measurement was conducted with a voltage of 40.0 kV, a current of 30.0 mA, and a scanning speed of 4.0 degrees per minute. The electrical conductivities were tested by a standard two-probe method using a source meter (Agilent E4980A). The samples were cut into strips with a width of 3 mm and a length of 3−4 cm. Then, the two sides were fixed by silver paste for better contact with the probe. FTIR was obtained by a Thermo Nicolet Nexus-470 FTIR instrument with the attenuated total reflection mode (ATR). Each specimen was tested at three different points.

Conflict of Interest: The authors declare no competing financial interest.

Acknowledgment. This work was supported by the Excellent Young Scientist Foundation of NSFC (51522301), the National Natural Science Foundation of China (21273017, 51103004), Program for New Century Excellent Talents in University (NCET-12-0034), Beijing Nova Program (Z121103002512020), Fok Ying-Tong Education Foundation (141045), Open Project of Beijing National Laboratory for Molecular Sciences, the 111 Project (B14009), Aeronautical Science Foundation of China (20145251035), State Key Laboratory for Modification of Chemical Fibers and Polymer Materials, Donghua University (LK1508), and the Fundamental Research Funds for the Central Universities (YWF-15-HXXY-001).

Supporting Information Available: The Supporting Information is available free of charge on the ACS Publications website at DOI: 10.1021/acsnano.5b02902.

Additional figures and tables (PDF)

REFERENCES AND NOTES

1. Park, S.; Ruoff, R. S. Chemical Methods for the Production of Graphenes. *Nat. Nanotechnol.* **2009**, *4*, 217–224.
2. Cheng, Q.; Duan, J.; Zhang, Q.; Jiang, L. Learning from Nature: Constructing Integrated Graphene-Based Artificial Nacre. *ACS Nano* **2015**, *9*, 2231–2234.
3. Cheng, Q.; Jiang, L.; Tang, Z. Bioinspired Layered Materials with Superior Mechanical Performance. *Acc. Chem. Res.* **2014**, *47*, 1256–1266.
4. Dikin, D. A.; Stankovich, S.; Zimney, E. J.; Piner, R. D.; Dommett, G. H. B.; Evmenenko, G.; Nguyen, S. T.; Ruoff, R. S. Preparation and Characterization of Graphene Oxide Paper. *Nature* **2007**, *448*, 457–460.
5. Yao, H.-B.; Ge, J.; Mao, L.-B.; Yan, Y.-X.; Yu, S.-H. 25th Anniversary Article: Artificial Carbonate Nanocrystals and Layered Structural Nanocomposites Inspired by Nacre: Synthesis, Fabrication and Applications. *Adv. Mater.* **2014**, *26*, 163–188.
6. Liu, R.-Y.; Xu, A.-W. Byssal Threads Inspired Ionic Cross-Linked Narce-Like Graphene Oxide Paper with Superior Mechanical Strength. *RSC Adv.* **2014**, *4*, 40390–40395.
7. Park, S.; Lee, K.-S.; Bozoklu, G.; Cai, W.; Nguyen, S. T.; Ruoff, R. S. Graphene Oxide Papers Modified by Divalent Ions—Enhancing Mechanical Properties *via* Chemical Cross-Linking. *ACS Nano* **2008**, *2*, 572–578.
8. Hu, K.; Tolentino, L. S.; Kulkarni, D. D.; Ye, C.; Kumar, S.; Tsukruk, V. V. Written-In Conductive Patterns on Robust Graphene Oxide Biopaper by Electrochemical Microstamping. *Angew. Chem., Int. Ed.* **2013**, *52*, 13784–13788.
9. Li, Y.-Q.; Yu, T.; Yang, T.-Y.; Zheng, L.-X.; Liao, K. Bio-Inspired Nacre-like Composite Films Based on Graphene with Superior Mechanical, Electrical, and Biocompatible Properties. *Adv. Mater.* **2012**, *24*, 3426–3431.
10. Putz, K. W.; Compton, O. C.; Palmeri, M. J.; Nguyen, S. T.; Brinson, L. C. High-Nanofiller-Content Graphene Oxide-Polymer Nanocomposites *via* Vacuum-Assisted Self-Assembly. *Adv. Funct. Mater.* **2010**, *20*, 3322–3329.
11. An, Z.; Compton, O. C.; Putz, K. W.; Brinson, L. C.; Nguyen, S. T. Bio-inspired Borate Cross-Linking in Ultra-Stiff Graphene Oxide Thin Films. *Adv. Mater.* **2011**, *23*, 3842–3846.
12. Gao, Y.; Liu, L.; Zu, S.; Peng, K.; Zhou, D.; Han, B.; Zhang, Z. The Effect of Interlayer Adhesion on the Mechanical Behaviors of Macroscopic Graphene Oxide Papers. *ACS Nano* **2011**, *5*, 2134–2141.
13. Cheng, Q.; Wu, M.; Li, M.; Jiang, L.; Tang, Z. Ultratough Artificial Nacre Based on Conjugated Cross-Linked Graphene Oxide. *Angew. Chem., Int. Ed.* **2013**, *52*, 3750–3755.
14. Tian, Y.; Cao, Y.; Wang, Y.; Yang, W.; Feng, J. Realizing Ultrahigh Modulus and High Strength of Macroscopic Graphene Oxide Papers Through Crosslinking of Mussel-Inspired Polymers. *Adv. Mater.* **2013**, *25*, 2980–2983.
15. Cui, W.; Li, M.; Liu, J.; Wang, B.; Zhang, C.; Jiang, L.; Cheng, Q. A Strong Integrated Strength and Toughness Artificial Nacre Based on Dopamine Cross-Linked Graphene Oxide. *ACS Nano* **2014**, *8*, 9511–9517.
16. Zhang, M.; Huang, L.; Chen, J.; Li, C.; Shi, G. Ultratough, Ultrastrong, and Highly Conductive Graphene Films with Arbitrary Sizes. *Adv. Mater.* **2014**, *26*, 7588–7592.
17. Jackson, A.; Vincent, J.; Turner, R. The Mechanical Design of Nacre. *Proc. R. Soc. London, Ser. B* **1988**, *234*, 415–440.
18. Wegst, U. G. K.; Bai, H.; Saiz, E.; Tomsia, A. P.; Ritchie, R. O. Bioinspired Structural Materials. *Nat. Mater.* **2014**, *14*, 23–36.
19. Wan, S.; Li, Y.; Peng, J.; Hu, H.; Cheng, Q.; Jiang, L. Synergistic Toughening of Graphene Oxide−Molybdenum Disulfide−Thermoplastic Polyurethane Ternary Artificial Nacre. *ACS Nano* **2015**, *9*, 708–714.
20. Rinaudo, M. Chitin and chitosan: Properties and Applications. *Prog. Polym. Sci.* **2006**, *31*, 603–632.
21. Yao, H. B.; Tan, Z. H.; Fang, H. Y.; Yu, S. H. Artificial Nacre-Like Bionanocomposite Films from the Self-Assembly of Chitosan-Montmorillonite Hybrid Building Blocks. *Angew. Chem., Int. Ed.* **2010**, *49*, 10127–10131.
22. Yang, X.; Tu, Y.; Li, L.; Shang, S.; Tao, X. M. Well-Dispersed Chitosan/Graphene Oxide Nanocomposites. *ACS Appl. Mater. Interfaces* **2010**, *2*, 1707–1713.
23. Podsiadlo, P.; Kaushik, A. K.; Arruda, E. M.; Waas, A. M.; Shim, B. S.; Xu, J.; Nandivada, H.; Pumplin, B. G.; Lahann, J.; Ramamoorthy, A.; et al. Ultrastrong and Stiff Layered Polymer Nanocomposites. *Science* **2007**, *318*, 80–83.
24. Tang, Z.; Kotov, N. A.; Magonov, S.; Ozturk, B. Nanostructured Artificial Nacre. *Nat. Mater.* **2003**, *2*, 413–418.

25. Walther, A.; Bjurhager, I.; Malho, J.-M.; Pere, J.; Ruokolainen, J.; Berglund, L. A.; Ikkala, O. Large-Area, Lightweight and Thick Biomimetic Composites with Superior Material Properties *via* Fast, Economic, and Green Pathways. *Nano Lett.* **2010**, *10*, 2742–2748.
26. Walther, A.; Bjurhager, I.; Malho, J.-M.; Ruokolainen, J.; Berglund, L.; Ikkala, O. Supramolecular Control of Stiffness and Strength in Lightweight High-Performance Nacre-Mimetic Paper with Fire-Shielding Properties. *Angew. Chem., Int. Ed.* **2010**, *49*, 6448–6453.
27. Das, P.; Malho, J.-M.; Rahimi, K.; Schacher, F. H.; Wang, B.; Demco, D. E.; Walther, A. Nacre-mimetics with Synthetic Nanoclays Up to Ultrahigh Aspect Ratios. *Nat. Commun.* **2015**, *6*, 5967.
28. Zhu, B. L.; Jasinski, N.; Benitez, A.; Noack, M.; Park, D.; Goldmann, A. S.; Barner-Kowollik, C.; Walther, A. Hierarchical Nacre Mimetics with Synergistic Mechanical Properties by Control of Molecular Interactions in Self-Healing Polymers. *Angew. Chem., Int. Ed.* **2015**, *54*, 8653–8657.
29. Brinker, C. J.; Scherer, G. W. Sol-Gel Science: the Physics and Chemistry of Sol-Gel Processing. In *Sol-Gel Science: The Physics and Chemistry of Sol-Gel Processing*; Academic Press, Inc.: San Diego, CA, 1990; pp 357−403.
30. Fang, M.; Long, J.; Zhao, W.; Wang, L.; Chen, G. pH-Responsive Chitosan-Mediated Graphene Dispersions. *Langmuir* **2010**, *26*, 16771–16774.
31. Fritz, G.; Schädler, V.; Willenbacher, N.; Wagner, N. J. Electrosteric Stabilization of Colloidal Dispersions. *Langmuir* **2002**, *18*, 6381–6390.
32. Napper, D. H. Steric Stabilization. *J. Colloid Interface Sci.* **1977**, *58*, 390–407.
33. Napper, D. H. Polymeric Stabilization of Colloidal Dispersions. In *Polymeric Stabilization of Colloidal Dispersions*; Academic Press, Inc.: London, 1983; pp 18−30.
34. Li, D.; Müller, M. B.; Gilje, S.; Kaner, R. B.; Wallace, G. G. Processable Aqueous Dispersions of Graphene Nanosheets. *Nat. Nanotechnol.* **2008**, *3*, 101–105.